Wave Propagation on MESFET Electrodes and Its Influence on Transistor Gain

WOLFGANG HEINRICH, MEMBER, IEEE, AND HANS L. HARTNAGEL, SENIOR MEMBER, IEEE

Abstract—A rigorous analysis of wave propagation along MESFET electrodes is presented. Both the losses caused by the channel and those caused by the finite electrode conductivity are included, together with small-signal amplification. Results from this wave analysis are used to determine overall gain. Conclusions concerning traveling-wave FET design, optimal gate width, and related criteria are drawn.

I. Introduction

In recent years, the MESFET has been used for a growing number of high-frequency amplifier applications. The frequency limits have been extended systematically; recently, for instance, a 6.5-dB gain at 60 GHz was reported [1].

When increasing the frequency, the dimensions of the transistor, in particular the so-called gate width, become more and more comparable to the wavelength. In this case, wave characteristics influence the electrical performance significantly, as is well known from passive waveguides. Consequently, the FET then must be modeled by distributed elements. The common MESFET equivalent circuits, however, use only lumped elements. Therefore, the question arises, up to which frequency and dimensional limits the simple lumped model is suitable. This discussion requires a fundamental study of wave propagation. Obviously, propagation effects occur mainly along the electrodes, since the unit finger gate width W is very large compared to source–drain spacing.

The same type of analysis is needed, of course, when designing the MESFET as a distributed amplifier, the so-called traveling wave FET (TWFET) [2]–[4]. Most authors, however, adopt too simple an equivalent circuit for the analysis, neglecting important effects such as losses [4]. The full-wave treatment presented here (see Section II) does not suffer from those weak points.

Based on the field-theoretical investigations described here, the authors developed also a distributed equivalent circuit model, which will be published elsewhere. Comparing results from distributed modeling with corresponding ones from lumped-element modeling, the errors due to the latter approximation can be calculated [14]. These results prove *a posteriori* the necessity of an analysis as undertaken in the following.

The paper is structured as follows: In Section II, a rigorous full-wave analysis of wave propagation along FET-electrodes is presented. The results from Section II are then used to determine the terminal gain of the FET (Section III) and discuss some important mechanism (Sections IV and V).

Manuscript received March 7, 1986; revised July 5, 1986. This work was supported in part by the Deutsche Forschungsgemeinschaft.

The authors are with the Institut für Hochfrequenztechnik, Technische Hochschule Darmstadt, 6100 Darmstadt, West Germany.

IEEE Log Number 8611023.

II. Wave Propagation Analysis

A. The Model

Fig. 1(a) shows a typical cross-sectional MESFET view. Most authors treating FET wave propagation model this configuration by quite simple equivalent circuits [4]–[6]. Recently some publications appeared analyzing similar structures, namely Schottky contact lines [7]–[10]. But only Itoh *et al.* [8], [9] assume nonzero electrode thickness, and none of them includes electrode losses. Heinrich and Hartnagel started their investigations with a passive FET model [11] and then developed a more detailed model including semiconductor and gate electrode losses, small-signal amplification, and partly, the losses on source and drain [12]. The latter treatment has now been enhanced again and the total losses on source and drain electrodes are taken into account (see Fig. 1(b)).

Using the same type of approach [11], [12], the whole structure is placed in a box with electric and magnetic walls in order to permit the use of the efficient method of orthogonal expansion. The magnetic walls at $x = 0, b$ simulate a periodic continuation in the x direction, as used in common FET's with several parallel electrode sets. Note that there is no connection from source to substrate metallization at $y = -a_2$. In order to restrain the numerical efforts, w_1 and w_3 must be chosen as small as possible. All regions are assumed arbitrarily conductive with complex

$$\epsilon_l = \epsilon_{rl}\epsilon_0 - j\frac{\kappa_l}{\omega}. \tag{1}$$

Regarding the values for κ_l, a problem arises when determining the conductivity κ_3 of the channel. The n-doped semiconductor conductivity may in general be calculated by using $\kappa = e \cdot \mu_n \cdot n_D$, with e the electronic charge, μ_n the mobility, and n_D the doping concentration.

0018-9480/87/0100-0001$01.00 ©1987 IEEE

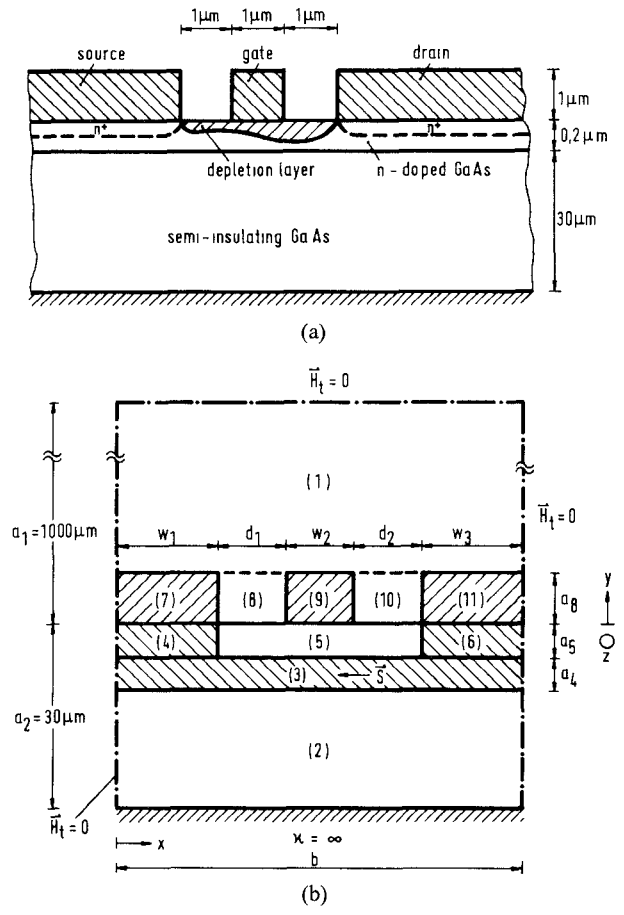

Fig. 1. (a) Cross-sectional view of a MESFET and (b) the corresponding waveguide model. Unless otherwise specified, the dimensions and material constants are as follows: $w_1 = w_3 = 4\ \mu m$; $w_2 = d_1 = d_2 = 1\ \mu m$; $a_4 = a_5 = 0.1\ \mu m$; $a_8 = 1\ \mu m$; $\vec{S}$ in region 3 $\sim g_m \cdot U_{GS}$ (see eq. (2)); $\epsilon_{r1} = \epsilon_{r7 \cdots 11} = 1$; $\epsilon_{r2 \cdots 6} = 12.9$; $\mu = \mu_0$ in all regions; $\kappa_t = 0$ except for the following: $\kappa_3 = 200\ (\Omega \cdot m)^{-1}$; $\kappa_4 = \kappa_6 = 2 \times 10^5\ (\Omega \cdot m)^{-1}$; $\kappa_7 = \kappa_9 = \kappa_{11} = 3 \times 10^7\ (\Omega \cdot m)^{-1}$.

For low-field conditions, the mobility of the relevant area of Fig. 1(b) is constant. Therefore, one finds a conductivity of $\kappa_4 = \kappa_6 \cong 2 \cdot 10^5\ (\Omega \cdot m)^{-1}$ in regions 4 and 6. In the channel (region 3), however, the static electric field, caused by the bias conditions, can exceed the low-field range in the high-field area near the drain-side end of the gate. There, the actual mobility decreases strongly. For the channel conductivity κ_3, therefore, an average value must be used for the analysis. Regarding common small-signal models, one finds a drain–source resistance R_{DS} between 200 and 500 Ω (e.g., [3]). That corresponds to κ_3 being in the range of 500–200 $(\Omega \cdot m)^{-1}$. In contrast to this, a low-field mobility of $\mu_n = 8500\ cm^2\ (V \cdot s)^{-1}$ and a channel doping of $1.5 \cdot 10^{17} cm^{-3}$ would give $\kappa_3 = 20\ 000\ (\Omega \cdot m)^{-1}$. To study this influence, the diagrams in Fig. 3 contain three different κ_3 values from 200 to 20 000 $(\Omega \cdot m)^{-1}$. The channel conductive behavior, of course, can be described more realistically, for example, by dividing region 3 into a source-side and a drain-side part with different conductivities. Such arrangements, however, cause severe additional efforts in theory and numerical computations. That is why the authors had to apply the more simple version described above.

The active behavior of the FET is modeled by an additional current density $\vec{S}$ in the channel (region 3). Applying a small-signal theory, $\vec{S}$ is modulated linearly by the gate–source voltage U_{GS}. For a detailed discussion, see [12, sec. III]. In principle, the additional current density $\vec{S}$ from drain to source corresponds to the RF current source with $I_{DS} = g_m \cdot U_{GS}$, as is well known from common equivalent circuits. Merely one extension is necessary: I_{DS} is transformed into terms of the electric and magnetic fields. With g_m being the *distributed* transconductance, the following holds:

$$\frac{\Delta(I_{DS})}{\Delta z} = -\int_{-a_5-a_4}^{-a_5} S_x|_{x=w_1}\, dy = g_m \cdot U_{GS},$$

$$\text{with } U_{GS} = -\int_0^{b/2} E_x|_{y=0}\, dx. \quad (2)$$

The distribution of $\vec{S}$ must fulfill the boundary conditions of region 3. Hence, in contrast to [12], a Fourier expansion is needed to determine $\vec{S}_{(x,y,z)}$ completely.

To avoid misunderstanding, two points should be outlined.

1) $\vec{S}$ represents a current density *additional* to the fields of the passive waveguide. The latter ones are superposed on the fields induced by $\vec{S}$.

2) The x direction dimensions are very small compared to wavelength. Consequently, in this analysis, the inhomogeneities in the channel may be well approximated by average values. This assumption, of course, would not be valuable if, for instance, carrier transport phenomena are to be studied.

B. Method of Analysis

Since there are regions with $0 < \kappa_t < \infty$ and active properties, in particularly in view of the electrode losses [13], the analysis presented here employs a mode-matching technique [8], [11], [12] (for further details see [12, sec. IV]). Due to the very detailed structure, the computer program consumes a relatively large value of CPU time. Calculating a typical example of a propagation constant and the corresponding field amplitudes with 1-percent accuracy requires about 800 s on the IBM 370/168 of the Technische Hochschule Darmstadt.

C. Results from the Wave Propagation Analysis

The waveguide in Fig. 1(b) supports three fundamental modes, namely, gate, drain, and bulk mode. Fig. 2 illustrates their characteristics. Since for $g_m = 0$ the whole structure is symmetrical to $x = b/2$. odd and even modes may be defined in that case (Fig. 2(a)).

With $g_m > 0$, the field distribution of the gate mode changes basically as shown in Fig. 2(b). This effect can be explained as follows. At $g_m = 0$, the gate mode represents an odd mode. With $g_m > 0$, the odd-mode fields induce the additional current density $\vec{S}$ in region 3. $\vec{S}$ possesses an *even*-mode distribution. Hence, when increasing g_m, more and more additional *even*-mode fields are created, which superpose the original *odd*-mode fields and cause the principal change from Fig. 2(a) to (b).

The bulk mode exhibits simple guided-wave characteristics, with $\beta/\beta_0 = 3.6 \approx \sqrt{\epsilon_{r2}}$ and $\alpha \ll \beta$ in the usual

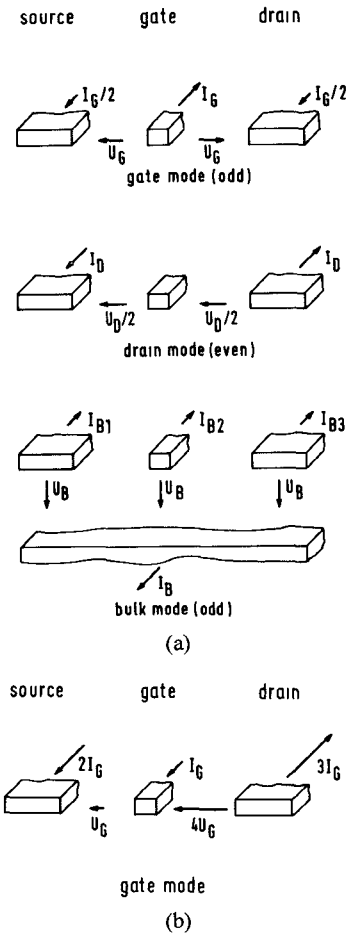

Fig. 2. The current and voltage characteristics of the three fundamental modes. (a) At $g_m = 0$. (b) Gate mode at $g_m = 100$ mS/mm, $\kappa_3 = 200$ $(\Omega \cdot \mathrm{m})^{-1}$, $f = 10$ GHz.

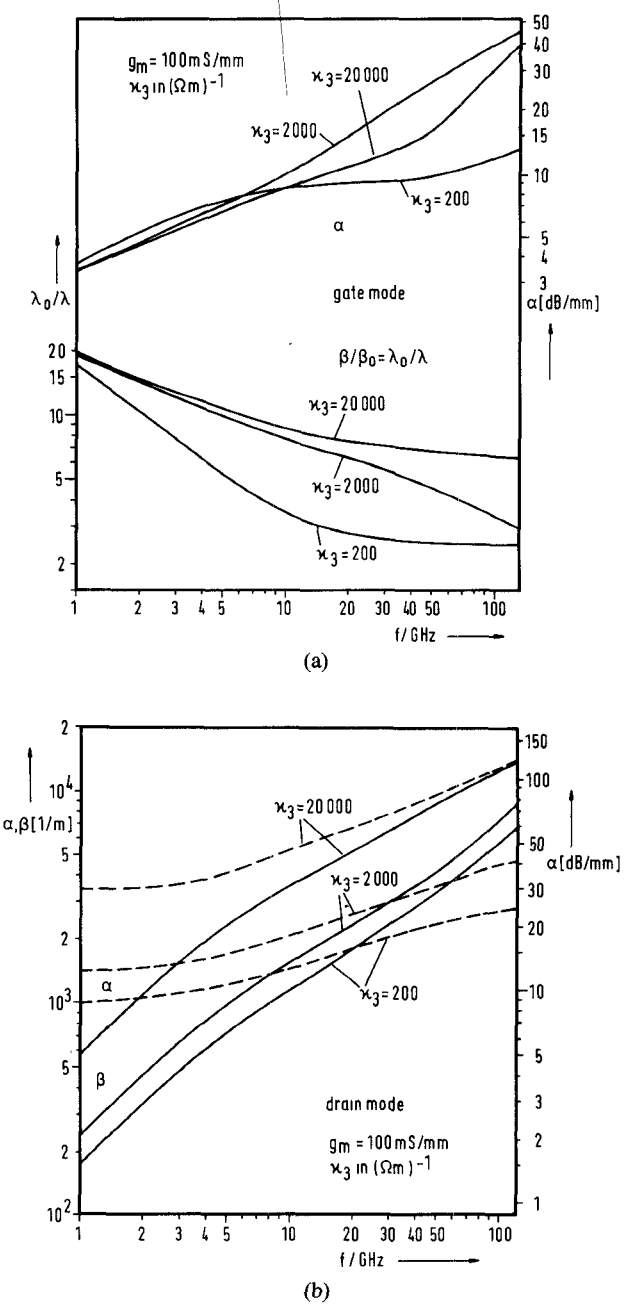

Fig. 3. Propagation constants of the gate and drain mode as a function of frequency f at different κ_3 values.

frequency range. For this reason, any special graphic presentation was omitted.

Higher order modes have been found but are of no interest, since their cutoff frequencies are very high and their propagation behavior is determined more by the box dimensions than by the planar electrode structure.

The results for gate and drain mode are plotted in Figs. 3–5. Wave propagation $\sim \exp(-jk_z z)$ with $k_z = \beta - j\alpha$ is considered. Fig. 3 shows the frequency dependence of β and α at different κ_3 values (see Section II-A); Figs. 4 and 5 show the influence of distributed transconductance g_m and electrode conductivity κ_{EL}, respectively. Concerning the latter diagram, one has to add that conductivity values of 10^8 $(\Omega \cdot \mathrm{m})^{-1}$ and more are not realizable. Nevertheless, these curves are helpful in clarifying the principal behavior. Variation of other parameters was applied but did not lead to a new understanding.

Some important statements can be made now.

1) The gate-mode propagation behavior is governed by the gate electrode losses and the fields in the depletion layer beneath the gate. The latter point becomes obvious at frequencies beyond 10 GHz (see Fig. 3(a), $\kappa_3 = 20\ 000$ $(\Omega \cdot \mathrm{m})^{-1}$) and at high electrode conductivities (see Fig. 5), where slow-wave-like properties can be found with $\beta/\beta_0 \approx 7$. That fits the results well derived previously [11], [12].

2) The drain-mode behavior is that of a guided wave attenuated drastically by the transverse currents in the channel (region 3). At frequencies below 20 GHz, additionally the electrode losses on source and drain exert a strong influence, producing $\alpha > \beta$ (see Fig. 3(b)). The treatment in [12] neglects these losses almost totally and therefore gives wrong results for lower frequencies. This is the main reason why the model of [12] was improved.

3) In spite of the differences mentioned above, the propagation constants of the two modes are of the same order. Furthermore, it must be underlined that the attenuation values are very high. Therefore, when analyzing wave propagation, low-loss approximations must not be adopted (as done, for instance, in [4] and [6]).

4) Regarding Fig. 4, it may be surprising that the transconductance g_m is associated with additional drain-

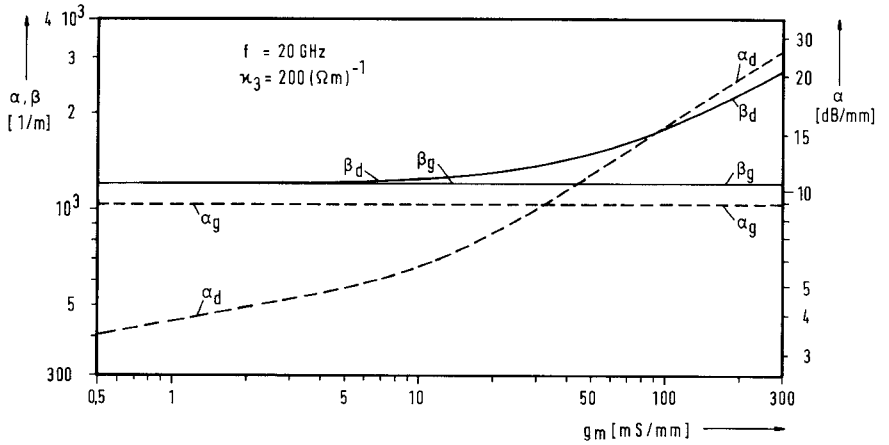

Fig. 4. Propagation constants of the gate and drain mode as a function of transconductance g_m at $f = 20$ GHz, $\kappa_3 = 200\ (\Omega \cdot \mathrm{m})^{-1}$.

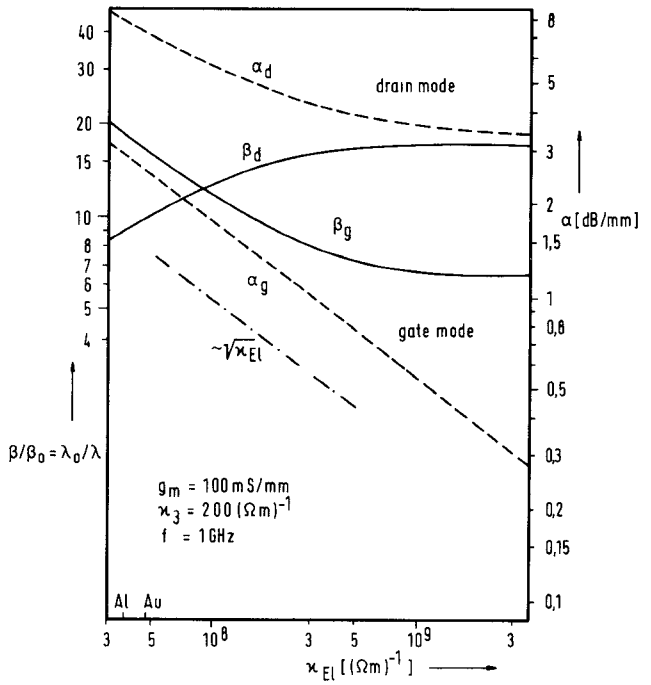

Fig. 5. Propagation constants of the gate and drain mode as a function of electrode conductivity $\kappa_{EL} = \kappa_7 = \kappa_9 = \kappa_{11}$ at $f = 1$ GHz, $\kappa_3 = 200\ (\Omega \cdot \mathrm{m})^{-1}$ (the values for gold and aluminum are marked).

mode losses and no reduction of α takes place. This behavior depends on the correlation between inductive and capacitive/conductive coupling from drain to gate.

More generally, we found that the usual FET structures support *no* growing waves! This rule can be altered merely by major modifications of the device, as done, for instance, in [2].

An important question for further investigations has still to be answered: Are the simple voltage and current definitions

$$U_{is} = -\int_{\text{source}}^{\text{conductor } i} \vec{E} \cdot d\vec{S} \quad \text{and} \quad I_{zi} = \oint_{C_i} \vec{H} \cdot d\vec{S} \tag{3}$$

(where U_{is} is the voltage conductor i referred to source, I_{zi} is the current conductor i in z direction, and C_i is the

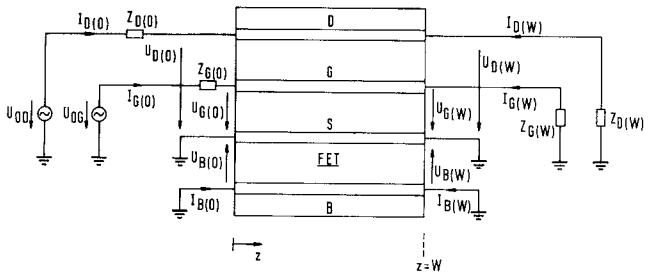

Fig. 6. The FET and its terminal network (most general case). The FET cross section is shown in Fig. 1; "B" indicates substrate metallization.

contour of conductor i) valid in the parameter range under consideration? Two quantities providing information about their validity were calculated from the computer analysis:

$$\Delta P = \left| \left(P_z - \frac{1}{2} \sum_{i=1}^{3} U_{is} I_{zi}^* \right) / P_z \right|$$

$$\Delta I = \frac{\left| \sum_{i=1}^{4} I_{zi} \right|}{1/2 \sum_{i=1}^{4} |I_{zi}|} \tag{4}$$

where U_{is} and I_{zi} are obtained from (3) and P_z is the power transported in the $+z$ direction (calculated from the fields by means of the complex Poynting vector). ΔI and ΔP were found to be less than 1 percent from 0.3 to 100 GHz for the parameter set of Fig. 1. Thus, the definition of (3) holds with good accuracy. This detail is essential for the further treatment in Section III as much as for effective modeling.

III. The Overall Performance

The overall performance (power gain, S-matrix, impedance matrix) has to be used when characterizing transistor properties. In this way, a suitable procedure was applied to transform the wave characteristics (from Section II) to the terminal performance quantities of the whole setup in Fig. 6. Thus, for example, the scattering matrix of a device with

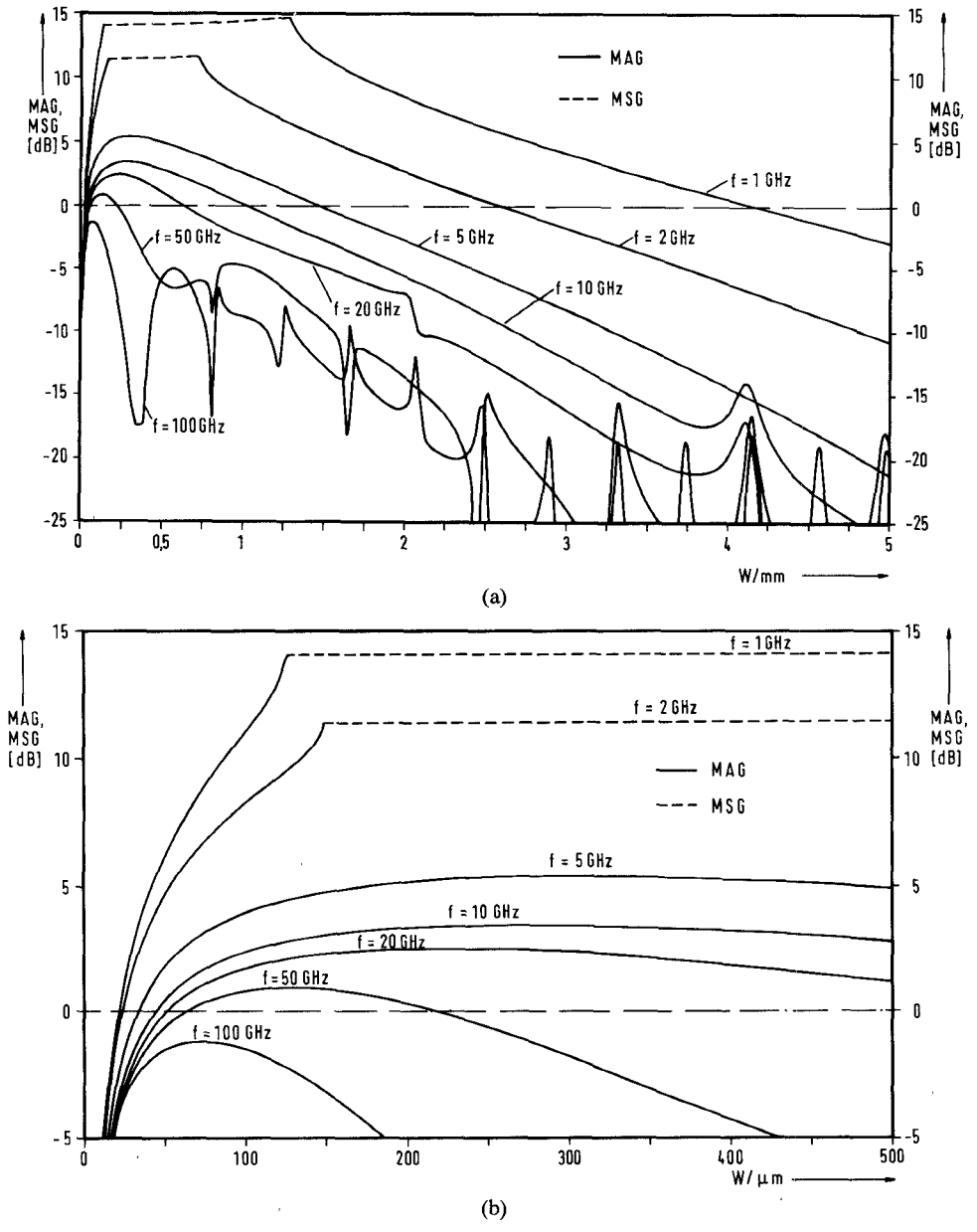

Fig. 7. Maximum available gain MAG (——) and maximum stable gain MSG (---) for the conditionally unstable device as a function of the gate width W at different frequencies f (FET parameters as given in Fig. 1, $Z_{G(W)} = Z_{D(0)} = 1\ \text{k}\Omega$).

wave propagation characteristics as outlined above can be computed.

Assuming that voltages and currents I_z are well defined ((3) and (4)), that the higher order modes can be neglected, and that the termination conditions can be described by voltages and currents, including the limit of open-ended electrodes, the impedance matrix (z) is derived from the fields and propagation constants of the three fundamental modes (see Appendix). After introducing the termination conditions at $z = 0$ and $z = W$, gain and all other quantities of interest may be calculated by means of common network theory.

In the following, two device characteristics shall be considered: the maximum available gain, MAG, and the maximum stable gain, MSG (see, for example, [15]). At some values of gate width W and of frequency, no MAG can be defined, because the transistor under consideration is merely conditionally stable (the Rollett constant k is smaller than 1). In those cases, the MSG has been computed instead.

Unless otherwise specified, the input signal is fed to the gate at $z = 0$ and the load is connected to the drain at $z = W$. The remaining two ports (gate at $z = W$, drain at $z = 0$) are approximately open ended ($Z_{G(W)} = Z_{D(0)} = 1\ \text{k}\Omega \gg$ characteristic impedances). Exact open ending gives horizontal curves in Fig. 7 for $W \to 0$ but requires unrealistically high impedance matching of input and output to obtain the MAG and MSG, respectively. Extracting the output signal at $z = 0$ instead of $z = W$ causes some changes but does not affect the following considerations. It should

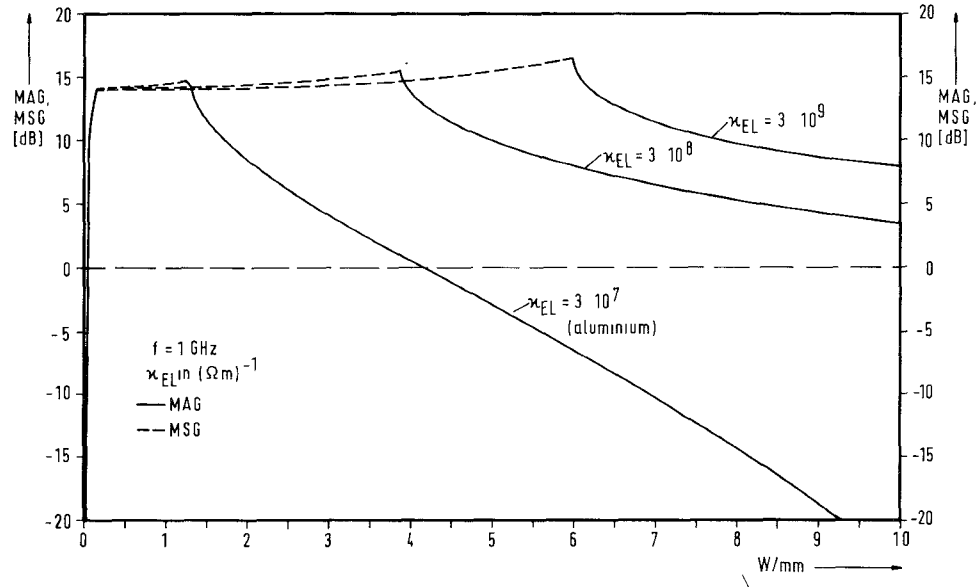

Fig. 8. MAG (——) and MSG (---), respectively, as a function of the gate width at different electrode conductivity values κ_{EL} ($f = 1$ GHz, κ_{EL} in $(\Omega \cdot m)^{-1}$, $Z_{G(W)} = Z_{D(0)} = 1\ k\Omega$).

be noted that in practice this point depends on the particular FET periphery. Therefore, no general rule can be observed.

A plot of MAG and, where this quantity is meaningless, of MSG as a function of the gate width W at different frequencies is presented in Fig. 7. The transconductance g_m was chosen to be frequency-independent to exclude carrier transport mechanisms, which will cause deviations at frequencies beyond ≈ 20 GHz for the given 1-μm gate length, and to concentrate only on the wave propagation phenomena.

IV. Optimum FET Parameters

In many cases, it is important to know at which gate width, W_{opt}, the highest possible gain can be achieved. W_{opt} varies in the range of several hundred micrometers at frequencies below 50 GHz (see Fig. 7). Fig. 7(b) shows the interesting details on a larger scale. One finds here good agreement with practical experience. It should be noticed that realizing input and output matching (as provided to achieve MAG) becomes more difficult if W is small because of high impedance levels.

Increasing W beyond W_{opt} reduces gain. From the wave analysis, one can assume that the losses, especially those of the electrodes, exert a strong influence on MAG degradation. To elucidate this point, the electrode conductivity was increased to (nonphysically) high values, as can be seen from Fig. 8. (Please note that only the gate-mode losses are reduced drastically; the drain mode remains quite unchanged (see Fig. 5).) Thus, gain features are improved and W_{opt} grows. Nevertheless, the descending part of the curves for long transistors is shifted but not altered.

Various proposals have been made in the literature to change device parameters (e.g., the FET cross-sectional geometry) in such a way as to optimize wave propagation and thus transistor gain [4], [6]. Since [12] was published, most of them seem to be questionable because of their low-loss approximations.

To probe further, several parameters of the FET structure (Fig. 1) were varied, and the MAG was studied (the channel conductivity κ_3, the n^+-layer conductivity ($\kappa_4 = \kappa_6$), the distributed transconductance g_m, the electrode thickness a_8, the dimensions of the depletion layer (a_4, a_5)). Higher g_m values, of course, achieve higher gain. But the remaining parameters listed above do not exert a significant influence on MAG, which increases only by a few dB when optimizing such parameter values in a realistic range. Although this is of interest for optimized lumped FET design, it offers no special TWFET features.

V. Matching Conditions

One may conclude from Section IV that the usual gate-in, drain-out configuration has to be altered and that wave characteristics should be included to avoid gain limitations. For example, we may assume that source, gate, and drain electrodes are matched by the wave impedances of a certain mode and fed with appropriate voltages at $z = 0$ such that only this particular mode is excited. Then this single mode would propagate in the positive z direction provided that longitudinal homogeneity exists so that no mode transformation occurs. Assuming single-mode propagation on the structure, one has

$$\frac{P_{out}}{P_{in}} = e^{-2\alpha_i W}$$

where α_i is the attenuation constant of mode i. Hence, for attenuated waves ($\alpha_i > 0$), no gain can be obtained at all.

The main disadvantage of such an FET amplifier is the fact that there is no gain unless growing waves exist. Since the common FET's do not support growing waves (see Section II-C), new structures would have to be developed,

which, for instance, provide a positive (!) feedback from drain to gate or adopt modifications as proposed in [2]. On the other hand, because of the nondirectional device, the existence of growing waves would result in severe instabilities. Furthermore, problems arise in realizing the correct matching circuits. They are of great complexity, especially if broad-band features are desired.

A second point concerning this topic shall be mentioned. At frequencies above 5 GHz, sharp peaks occur in the MAG curves (see Fig. 7). These peaks are caused by the bulk mode (Fig. 2), more strictly speaking, by the fact that the source electrode is usually only grounded to the substrate metallization at the ends of the FET (except where systematic via-hole grounding is used).

VI. Conclusions

The results of the analysis presented in Sections II and III are of special interest for the following two cases.

1) *Modeling of Existing FET Devices*: Some state-of-the-art MESFET's are operating at frequencies where, depending on the gate width, wave propagation effects significantly influence their performance (see [14]). In most practical cases, the need arises for a simplified model, one that approximates the theoretical results as well as necessary and can be handled more easily. Because of the small values of ΔI and ΔP found above (see (4) in Section II-C), modeling by (distributed) equivalent circuits seems to be suitable. It must be pointed out here that a simple $L-C$ traveling-wave configuration (e.g., [4], [6]) is not adequate and a version more appropriate to FET's must be used. Especially, one cannot neglect electrode and channel losses or the inductive and capacitive coupling. Low-loss assumptions or nonrealistic coupling will give erroneous results! Based on the theoretical investigations, the authors developed an appropriate equivalent circuit model, which is beyond the scope of this paper.

2) *Traveling-Wave FET's*: There are many experiments to achieve increased (broad-band) transistor gain by means of wave propagation effects along the electrodes. (Only nondiscrete distributed structures are considered here; configurations using discrete FET cells (e.g., [3]) are omitted in our discussion.) As can be seen from Section IV, FET parameter optimization without a major modification of the structure results in merely a few dB gain enhancement. Most proposals promising great improvement by only minor changes of geometry (e.g., [4], [6]) are misleading. In these cases, elongation of the FET structure does not improve gain; the optimum gate width remains small in comparison with the wavelength. Even the use of suitable matching for single wave-mode operation (as outlined in Section V) does not produce any gain increase. These results are therefore not promising for a nondiscrete TWFET amplifier.

Hence, it would be desirable to embark on a systematic study on FET structures supporting growing waves. As can be concluded from Section V, matching *and* the existence of a growing wave would give steady gain increase with gate width. On the other hand, instabilities due to mismatching are very difficult to avoid in such a TWFET and must be investigated thoroughly. Although this consideration therefore seems to be primarily a theoretical one given the present state of the art, it offers interesting guidelines for future work. Moreover, if such an arrangement is introduced gradually, the attenuation constant varies steadily from positive to negative values. That means there is a range where the losses are reduced but no growing waves exist. In this case, transistor gain is enhanced (see Fig. 8) without matching and severe instability problems, since the FET may be operated in the usual gate-in, drain-out configuration.

Appendix

Derivation of the FET Impedance Matrix

From the electric and magnetic fields obtained by the mode-matching technique, voltages and currents on the three electrodes and the substrate metallization can be calculated for each mode by (3). All these quantities possess the z dependence $\exp\{\pm jk_z z\}$. There are two waves for each mode i traveling in the positive and the negative z direction with the same propagation constant k_{zi} and the unknown amplitudes A_{i+}, A_{i-} respectively.

For further treatment, the following indices are used (all voltages are related to the source):

- G gate electrode,
- S source electrode,
- D drain electrode,
- B substrate metallization,
- g gate mode,
- d drain mode,
- b bulk mode.

$U_D^{(g)}$, for instance, means the drain–source voltage for the gate mode. One derives the voltages and currents at the six ports (see Fig. 6):

$$U_{m(z_0)} = \sum_{n=g,d,b} U_m^{(n)} \left\{ A_{n+} e^{-jk_{zn}z_0} + A_{n-} e^{+jk_{zn}z_0} \right\}$$

$$I_{m(z_0)} = \sum_{n=g,d,b} f_{(z_0)} \cdot I_m^{(n)} \left\{ A_{n+} e^{-jk_{zn}z_0} - A_{n-} e^{+jk_{zn}z_0} \right\} \tag{A1}$$

with $m = G, D, B$; $z_0 = 0, W$; and

$$f_{(z_0)} = \begin{cases} 1 & z_0 = 0 \\ -1 & z_0 = W. \end{cases}$$

Rewritten by matrix theory, the twelve equations (A1) reduce to

$$(U) = (M_U) \cdot (A)$$
$$(I) = (M_I) \cdot (A) \tag{A2}$$

where (U) contains the $U_{m(z_0)}$, (I) the $I_{m(z_0)}$, and (A) the A_{n+}, A_{n-}. (M_U) and (M_I) are matrices of order 6×6. Obviously, after eliminating (A), the impedance matrix (z) is

$$(z) = (M_U) \cdot (M_I)^{-1}. \tag{A3}$$

REFERENCES

[1] B. Kim, H. Q. Tserng, and H. D. Shih, "Millimeter-wave GaAs FETs prepared by MBE," *IEEE Electron Device Lett.*, vol. EDL-6, pp. 1–2, 1986.

[2] A. J. Holden, D. R. Daniel, I. Davies, C. H. Oxley, and H. D. Rees, "GaAs travelling-wave field-effect transistors," *IEEE Trans. Electron Devices*, vol. ED-32, pp. 61–66, Jan. 1985.

[3] K. B. Niclas, W. T. Wilser, T. R. Kritzer, and R. R. Pereira, "On theory and performance of solid-state microwave distributed amplifiers," *IEEE Trans. Microwave Theory Tech.*, vol. MTT-31, pp. 447–456, June 1983.

[4] A. S. Podgorski and L. Y. Wei, "Theory of travelling-wave transistors," *IEEE Trans. Electron Devices*, vol. ED-29, pp. 1845–1853, Dec. 1982.

[5] W. Jutzi, "Theorie zweier aktiv und passiv gekoppelter Leitungen," *Arch. Elek. Übertragung*, vol. 23, pp. 1–8, 1969.

[6] C. J. Wei, "Novel design of travelling-wave FET," *Electron. Lett.*, vol. 19, no. 13, pp. 461–462, June 1983.

[7] T. C. Mu, H. Ogawa, and T. Itoh, "Characteristics of coupled slow-wave microstrip lines," *Electron. Lett.*, vol. 21, no. 20, pp. 946–947, Sept. 1985.

[8] Y. Fukuoka, Y. C. Shih, and T. Itoh, "Analysis of slow-wave coplanar waveguide for monolithic integrated circuits," *IEEE Trans. Microwave Theory Tech.*, vol. MTT-31, pp. 567–573, July 1983.

[9] Y. Fukuoka and T. Itoh, "Analysis of slow-wave phenomena in coplanar waveguide on a semiconductor substrate," *Electron. Lett.*, vol. 18, no. 14, pp. 589–590, July 1982.

[10] R. Sorrentino and G. Leuzzi, "Full-wave analysis of integrated transmission lines on layered lossy media," *Electron. Lett.*, vol. 18, no. 14, pp. 607–608, July 1982.

[11] W. Heinrich and H. L. Hartnagel, "Wave-theoretical analysis of signal propagation on FET electrodes," *Electron. Lett.*, vol. 19, no. 2, pp. 65–67, Jan. 1983.

[12] W. Heinrich and H. L. Hartnagel, "Field-theoretic analysis of wave propagation on FET electrodes including losses and small signal amplification," *Int. J. Electron.*, vol. 58, no. 4, pp. 613–627, 1985.

[13] P. Waldow and I. Wolff, "The skin effect at high frequencies," *IEEE Trans. Microwave Theory Tech.*, vol. MTT-33, pp. 1076–1082, Oct. 1985.

[14] W. Heinrich, "On the limits of FET modelling by lumped elements," *Electron. Lett.*, vol. 22, no. 12, pp. 630–632, June 1986.

[15] R. S. Pengelly, *Microwave Field-Effect Transistors — Theory, Design and Applications*. Chichester, England: Research Studies Pr., 1982, ch. 5, pp. 143–147.

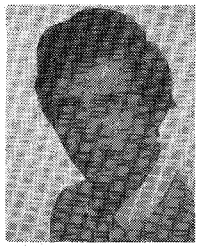

Wolfgang Heinrich (M'84) was born in Frankfurt am Main, West Germany, in 1958. He received the Dipl. Ing. degree from the Technical University of Darmstadt, West Germany, in 1982.

In January 1983, he joined the staff of the Institut für Hochfrequenztechnik of the same university as a research assistant, working also towards the doctoral degree. Since 1981, he has been involved with field-theoretical investigations and modeling of various FET electrode and stripline structures.

✠

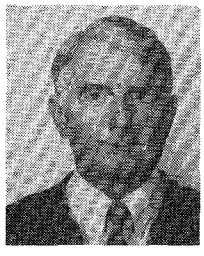

Hans L. Hartnagel (SM'72) was born in Geldern, Germany, in 1934. He received the Dipl. Ing. degree in 1960 from the Technical University of Aachen, Germany, and the Ph.D. and the Dr.Eng. degrees from the University of Sheffield, England, in 1964 and 1971, respectively.

After having worked for a short period with the company Telefunken in Ulm, Germany, he joined the Institut National des Sciences Appliquées, Villeurbanne, Rhône, France. He then joined the Department of Electronic and Electrical Engineering of the University of Sheffield. At first a Senior Research Assistant, in October 1962 he became a Lecturer and later was made a Senior Lecturer and Reader. From January 1, 1971, he held the position of Professor of Electronic Engineering at the University of Newcastle upon Tyne, England. Since October 1978, he has been a Professor of high-frequency electronics at the Technical University of Darmstadt, in West Germany.

Dr. Hartnagel is the author of books and numerous scientific papers, first on microwave tubes and then on microwave semiconductor devices, their technology, and their circuits. He has held many consulting positions, partly while on temporary leaves of absence from his university positions.